Non-Bragg resonance of surface water waves in a trough with periodic walls

Yumeng Xiao, Zhiyong Tao,* Weiyu He, and Xinlong Wang†
Key Laboratory of Modern Acoustics and Institute of Acoustics, Nanjing University, Nanjing 210093, People's Republic of China
(Received 12 March 2008; revised manuscript received 9 June 2008; published 22 July 2008)

The non-Bragg resonance of surface water waves is investigated, both theoretically and experimentally, in a trough with square-wave corrugated sidewalls. Unlike the familiar Bragg resonances, the non-Bragg resonances occur far from the edges of the Brillouin zone and open additional forbidden bands. The experimental observations confirm the existence of these resonances, and the measurements for the transmission properties showing both Bragg and non-Bragg band gaps agree fairly well with the theoretical predictions obtained by the plane-wave expansion method. It is shown that both Bragg and non-Bragg resonances highly depend on the symmetry of the corrugations on the opposite sidewall. As the relative shift between the two corrugations increases from zero to the half period of the corrugations, the Bragg gap shrinks and vanishes, but the non-Bragg gap varies in the opposite way, reaching its maximum, which is impressively wide and much more efficient in reflecting water waves.

DOI: 10.1103/PhysRevE.78.016311 PACS number(s): 47.90.+a, 47.35.−i, 68.05.−n, 92.10.Hm

I. INTRODUCTION

During past decades, wave propagation in periodic structures has been extensively investigated due to the physical aspects and potential applications of these structures, such as photonic [1,2] and phononic crystals [3,4], fiber grating sensors [5], and thermal management [6,7]. All this research focused on Bragg resonances caused by the periodicity, which opens the Bragg gap and leads to control over the band structure for special purposes. For instance, group velocity reduction [8] and negative refraction [9] can be realized near the Bragg gap. Recently, these concepts have been developed in water waves over periodic bottoms for applications in ocean engineering [10–21], as well as for a good demonstration of the physical concepts of wave propagations in periodic structures by direct observation of the phenomena with the naked eye [22–26].

In addition to Bragg resonances, non-Bragg resonances also play an essential role in the creation of band gaps in periodic waveguides. In 1998, Pogrebnyak studied the wave phenomena in a frequency range far from the Bragg resonances and predicted non-Bragg nature resonances in a sinusoidally corrugated planar electromagnetic waveguide [27]. Later, he investigated the controllability of band gaps induced by Bragg and non-Bragg resonances for electron waves in a quantum well with periodically corrugated walls [28] and for electromagnetic waves in a sinusoidally corrugated planar waveguide [29]. Unlike the Bragg resonances, the non-Bragg resonances arise away from the edges of the Brillouin zone with different transverse modes [30] and result in the creation of additional band gaps. With a change in the average thickness or the period, the location and width of band gaps can be adjusted from zero to a maximum value, and thus a tunable non-Bragg gap was predicted at the microwave range of frequency in a sinusoidally corrugated planar waveguide [31]. However, a detailed experimental investigation of the characteristics of non-Bragg gaps is still required to confirm the theoretical prediction. Also, approaches should be made to verify if such resonant phenomenon could be extended to other types of waves, such as water waves. To the author's knowledge, the concept of the non-Bragg resonance remains untouched in the context of water waves propagating in water channels, although there exists a rich literature on the Bragg resonance [32] and transverse mode coupling [33,34].

In this paper, we investigate water wave propagation in a trough with two square-wave corrugated sidewalls. Our attention is paid to the existence of the non-Bragg resonance in water waves and its properties in band gap formation. In the following section, we give a description of our experimental system, in particular, the structure of the periodic waveguide. Then, in Sec. III, a brief theoretical analysis is given to derive the dispersion relation for surface water waves with the plane-wave expansion method. The theory predicts the existence of a non-Bragg resonance and the dependency of the band structure on the relative shift of two sidewall corrugations. Section IV reports experimental observations that demonstrate these predictions. Also, some important results about the properties of the non-Bragg resonance are presented in detail. Finally, the main results are summarized in the concluding section.

II. DESCRIPTION OF THE EXPERIMENTAL SYSTEM

Our experimental setup is schematically illustrated in Fig. 1(a). We use a rectangular glass-walled trough 4000 mm long, 92 mm wide, and 300 mm high, filled with clean water of uniform depth h. On one end of the trough, a V780 vibrator (LDS Test & Measurement Ltd.) drives a piston to generate monochromatic plane water waves. On the other end, the transmitted wave is incident on and almost absorbed by a slanted sponge beach, with a slope of 1:10.

The periodic structure of the water channel implemented in this system is more clearly shown in Fig. 1(b). On the inner surface of each sidewall, a series of equally spaced identical blocks of glass are firmly fastened to form a corru-

*zytao@nju.edu.cn
†xlwang@nju.edu.cn

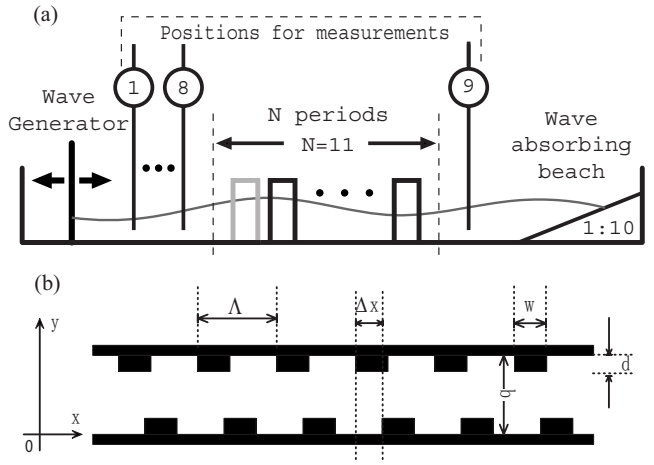

FIG. 1. (a) Schematic diagram of the experimental system (side view). (b) Part of the periodic structure (top view).

gation with period Λ. Each block is as high as the sidewalls, with thickness d less than half the channel breadth b, and width $w<\Lambda$, and the corrugations are identical on the opposite sidewalls, except for a longitudinal shift Δx. The relative shift can be measured by the dimensionless phase $\theta=K\Delta x$, where $K=2\pi/\Lambda$. By taking the (x,y) plane in Cartesian coordinates as shown in Fig. 1(b), and the z axis pointing in the upward direction perpendicular to the flat water surface at $z=0$, the actual sidewall profiles can be expressed as

$$y_1 = dY(Kx-\theta),$$

$$y_2 = b - dY(Kx), \tag{1}$$

with $Y(x)=Y(x+2\pi)$, and

$$Y(x) = \begin{cases} 1, & 0 < x \leqslant Kw, \\ 0, & Kw < x \leqslant 2\pi. \end{cases} \tag{2}$$

To measure the wave motion, a gauge is used to probe the surface elevations at nine points on the midline of the trough, as is indicated in Fig. 1(a). The gauge is a pair of (closely separated) parallel electrodes vertically dipped into water [10]. Owing to the reflection from the periodic structure, the wave ahead of the wave generator is partially standing. We separate the amplitude of the incident wave from that of the standing one by detecting the wave peaks and troughs, and measuring the corresponding amplitudes. This is accomplished by choosing a set of eight measurement positions, from 1 to 8, which are located on the up-wave side of the periodic corrugations, approximately midway between the corrugations and the piston. These positions are about 17 mm apart from each other on the midline, and they cover at least one wave peak and one trough. On the down-wave side of the periodic corrugations is the ninth measurement position at which the transmitted wave is recorded. Independent checks are carried out on the accuracy of the driving frequency f and the reflection coefficient of the slanted beach in the frequency range 2–6 Hz. The results indicate that the deviation of the working frequency is controlled within ± 0.005 Hz, and the reflection coefficient is smaller than 5%.

In the experiment, each wall corrugation contains $N=11$ periods, and the other dimensional parameters $w=40$ mm, $d=12$ mm, $b=92$ mm, $h=100$ mm, and $\Lambda=100$ mm. The period Λ is chosen such that the resonant frequency falls into the considered frequency range, within which surface water waves can be effectively excited and tested in the present system.

III. EXISTENCE OF THE NON-BRAGG RESONANCE

Before presenting our experimental observations, let us first give a brief theoretical analysis about surface wave propagation and their band structures in the above-described system. Under the assumptions of incompressible and inviscid fluid and irrotational motion, linear water waves in the waveguide of uniform depth h can be described by the velocity potential $\Phi(x,y,z,t)$ [10]. For the rigid boundary condition at $z=-h$ and the harmonic motion with an angular frequency $\omega=2\pi f$, $\Phi(x,y,z,t)$ can be expressed by the velocity potential on the bottom surface $\phi(x,y)$, as follows:

$$\Phi(x,y,z,t) = \phi(x,y)\cosh k(z+h)e^{-i\omega t} + \text{c.c.}, \tag{3}$$

where c.c. denotes the complex conjugate, and k is the wave number determined by the angular frequency ω through the linear dispersion relation [23]

$$\omega^2 = (gk + \gamma k^3/\rho)\tanh kh, \tag{4}$$

with g standing for the gravitational acceleration, $\gamma=73$ dyn/cm being the surface tension of clean water, and $\rho=1$ g/cm^3 the density of water. $\phi(x,y)$ is governed by the Helmholtz equation

$$\nabla^2\phi + k^2\phi = 0, \tag{5}$$

where the two-dimensional Laplace operator $\nabla^2=(\partial_x^2,\partial_y^2)$. It also satisfies the rigid boundary condition,

$$\frac{\partial\phi}{\partial\mathbf{n}} = \mathbf{0} \quad \text{at } y = y_1, y_2, \tag{6}$$

where $\mathbf{n}$ is an outward unit normal on the corrugated sidewalls.

According to Floquet's theorem [27], we have

$$\phi(x,y) = e^{i\beta x}u(x,y), \tag{7}$$

where β is the Bloch wave number and $u(x,y)=u(x+\Lambda,y)$ is a periodic function of x. Substituting it into Eq. (5) yields an expansion of $\phi(x,y)$:

$$\phi(x,y) = \sum_n (a_n e^{ik_{y,n}y} + b_n e^{-ik_{y,n}y})e^{ik_{x,n}x},$$

$$k_{x,n} = \beta + nK, \quad k_{y,n} = \sqrt{k^2 - k_{x,n}^2}, \quad n \in \mathbb{Z}, \tag{8}$$

where a_n and b_n are the coefficients of the Fourier series, and $k_{x,n}$ and $k_{y,n}$ are the longitudinal and transverse components of the wave number k, respectively.

Analogous to the earlier theoretical work [27,35], the Bragg and non-Bragg resonances occur at the intersections of the folded dispersion curves,

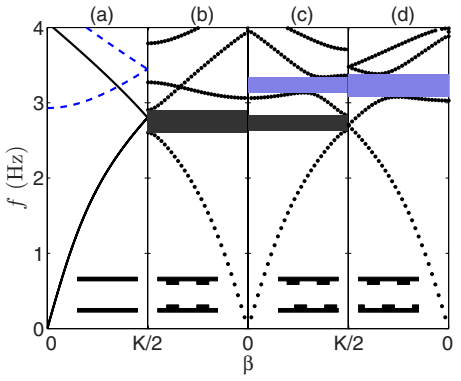

FIG. 2. (Color online) Dispersion curves for troughs with periodic units shown on the lower part of each subplot, (a) for a straight trough without corrugation; (b), (c), and (d) for troughs with phase shift $\theta=0$ (symmetric), $\pi/2$, and π (antisymmetric), respectively.

$$\beta_{pq} = \pm \frac{K}{2}\left\{1 - \left(\frac{\pi}{Kb}\right)^2 (p^2 - q^2)\right\}, \tag{9}$$

where p and q are the indices for different transverse modes [30], and the resonant frequency is defined as f_{pq}. For the Bragg resonance, the surface water waves have similar transverse distributions, i.e., $p=q$, and the resonant wave number $\beta_{pq}=\pm K/2$. So the Bragg resonances always occur at the edges of the Brillouin zone, while the non-Bragg resonances appear far away from the edges, with the surface waves having different transverse distributions, i.e., $p \neq q$.

Substituting Eq. (8) into the rigid boundary condition (6) and transferring them to the frequency regime leads to an infinite system of linear algebraic equations for the coefficient vectors $\mathbf{A}=\{a_n\}$, $\mathbf{B}=\{b_n\}$,

$$\mathbf{Q}\cdot\begin{bmatrix}\mathbf{A}\\ \mathbf{B}\end{bmatrix} = 0, \quad \mathbf{Q} = \begin{bmatrix}\mathbf{C}^{(+1)} & \mathbf{C}^{(-1)}\\ \mathbf{C}^{(+2)} & \mathbf{C}^{(-2)}\end{bmatrix}, \tag{10}$$

where $\mathbf{C}^{(\pm j)}=\{C_{m,n}^{(\pm j)}\}$ is an $m\times n$ matrix, $j=1,2$, and

$$C_{m,n}^{(\pm j)} = \int_0^{\Lambda} e^{-i(m-n)Kx}(\pm k_{y,n} - k_{x,n}y_j')e^{\pm ik_{y,n}y_j}dx. \tag{11}$$

The existence of nontrivial solutions to the coefficient vectors $\mathbf{A},\mathbf{B}$ requires that the determinant of the coefficient matrix $\mathbf{Q}$ must be zero,

$$\det\|\mathbf{Q}(k,\beta)\| = 0. \tag{12}$$

In the computation, the analytic expression of the integral in Eq. (11) is worked out and employed, and the infinite matrix $\mathbf{Q}(k,\beta)$ is truncated to a finite one by using $-M \leqslant m,n \leqslant M$. Here we choose $M=9$ to guarantee the satisfactory convergence of the eigenvalues. The accuracy is carefully checked by increasing M from 3 to 15. The discrepancy is less than 1%. Also the relevant geometrical parameters of the waveguide must be specified in the computation. Here we adopt those used in our experiment (see Sec. II).

The numerically calculated band structures for the troughs with four different arrangements are shown in Fig. 2. Due to the symmetry, only a half Brillouin zone with the width $K/2$ for each of the four cases is plotted, and they are arranged in sequence for direct comparison. Figure 2(a) presents the "folded" dispersion of the original trough without corrugation. The dispersions for the fundamental and the first transverse modes are shown by the solid and the dashed lines, respectively. For the trough used here, the first Bragg and non-Bragg resonances should occur at $f_{00}=2.80$ Hz and $f_{01}=3.20$ Hz, respectively. Also, another Bragg resonance appears at $f_{11}=3.42$ Hz, but it is noted that this resonance cannot result in a real complete gap because of the propagation of the fundamental mode. Figures 2(b)–2(d) show the dispersion curves (the black dots) and the forbidden bands (the shaded areas), respectively, at $\theta=0$, $\pi/2$, and π. For the symmetric case, i.e., $\theta=0$, a broad Bragg gap appears around the Bragg resonant frequency f_{00}, but the non-Bragg gap vanishes. On the contrary, for the antisymmetric case ($\theta=\pi$), the Bragg gap vanishes, and a wide non-Bragg gap emerges around the non-Bragg resonance frequency f_{01}. In the cases in between, such as $\theta=\pi/2$, there appear both band gaps, separated by a pass band, as can be seen in Fig. 2(c).

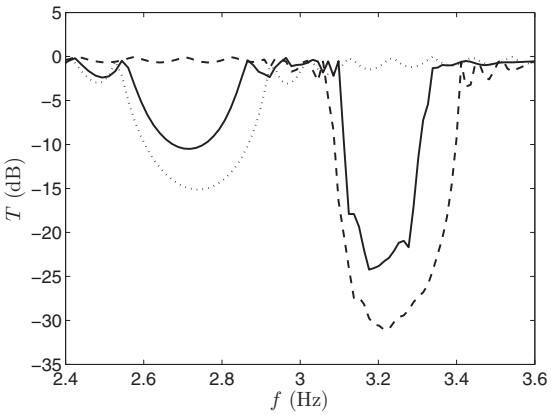

FIG. 3. Transmission coefficients (by simulations) of water waves through the periodic troughs for $\theta=0$ (dotted line), $\pi/2$ (solid line), and π (dashed line).

To investigate the effectiveness of prohibiting surface-wave propagations in the resonance-induced band gaps, the transmission coefficients T of the three periodic troughs just mentioned above are calculated directly from the Helmholtz equation (5) and the rigid boundary condition (6) with the finite-element method [36]. In the calculation, the damping effects are not taken into account. Here we restrict the periodic waveguide to be of finite length, and it contains the same number of periods as in experiment ($N=11$). Let a_{in} be the amplitude of the wave incident on the periodic structure, and a_{out} be the one transmitted through the periodic structure. Then the transmission coefficient is defined, as usual, by

$$T = 20\log_{10}\frac{a_{\text{out}}}{a_{\text{in}}}. \tag{13}$$

The numerical results are plotted in Fig. 3. For the symmetric and antisymmetric cases, either the Bragg (dotted line) or the non-Bragg (dashed line) gap results in the transmission loss ($-T$) through the periodic trough. In particular, the greater transmission loss is observed under the non-Bragg resonance, showing that the non-Bragg resonance is more

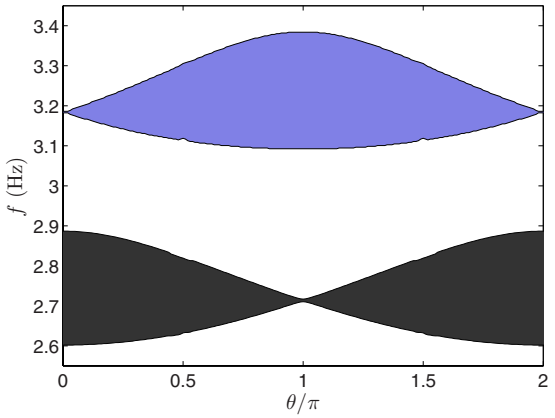

FIG. 4. (Color online) Band map as a function of the phase shift θ. The shaded areas denote the complete band gaps, the upper for the non-Bragg and the lower for the Bragg gap.

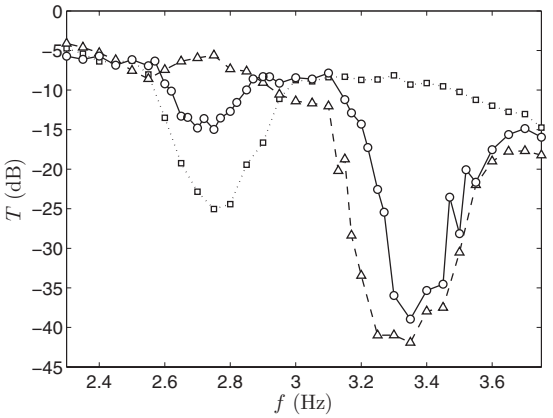

FIG. 5. Measured transmission coefficients T versus frequency, respectively, for $\theta=0$ (the squares connected by dotted line), $\pi/2$ (the circles connected by solid line), and π (the triangles connected by dashed line).

effective for damping surface water waves. For an intermediate case such as $\theta=\pi/2$ (solid line), the Bragg and non-Bragg gaps both cause transmission loss in the frequency range concerned, but the non-Bragg one still gives a greater transmission loss. All these forcefully demonstrate the crucial role the non-Bragg resonance plays in shaping the band gap structure of periodic troughs.

Further numerical results about the width of the two band gaps are plotted in Fig. 4. We map the position and the width of the band gaps as a function of the phase shift θ in the figure, and recognize the upper shaded area as the non-Bragg and the lower as the Bragg gap. It is clear that the Bragg gap narrows and the non-Bragg gap broadens as the phase shift θ increases from 0 to π. The optimal phase shift that gives a maximum sum width of the two gaps, $\Delta f=0.37$ Hz, is $\theta=\pi/2$.

In brief, we have predicted the existence of the non-Bragg resonance in a trough with periodic square-wave corrugated sidewalls, as long as there is a phase shift θ between the periodic corrugations of the opposite walls. The analysis also reveals that the non-Bragg-resonance-induced forbidden band can be as wide as the Bragg one. In particular, as the phase shift θ approaches π, i.e., the opposite corrugation becomes out of phase, the transmission loss within the non-Bragg gap can even be much greater than that in the Bragg gap.

IV. EXPERIMENTAL OBSERVATIONS AND RESULTS

To confirm these interesting findings and further investigate the properties of the non-Bragg resonances, we perform the experiment in the periodic trough described in Sec. II. In the experiment, a piston is driven to generate monochromatic plane water waves at the frequencies ranging from 2.30 to 3.75 Hz. To avoid nonlinear effects, the amplitudes a of generated water waves are controlled to be smaller than 10 mm (peak-peak value), so that $ka<0.2$. On the other hand, to ensure the sensitivity and precision of the measurement, the amplitudes of incident waves are sometimes adjusted to guarantee that the amplitudes of the transmitted waves are greater than 1 mm. As an exception, much larger-amplitude waves, namely, with 26 mm peak-peak value, which is the largest in the experiments, are produced at resonant frequencies, so as to detect the much weaker transmitted waves. Even for such large-amplitude incident waves, the transmitted wave is measured to be only about 0.1 mm in amplitude. We arrange the corrugations of the opposite sidewalls at three different phase shifts, $\theta=0$, $\pi/2$, and π. For each of the three geometrical configurations, the incident and transmitted wave amplitudes in the considered frequency range are recorded at the positions as described in Sec. II, and then the relative transmission coefficients along the center lines of the troughs can be calculated, as presented in Fig. 5. The results are in qualitative agreement with the theoretical ones in Fig. 3. In the symmetric case ($\theta=0$), the experiment confirms the existence of the Bragg gap but the nonexistence of the non-Bragg gap. For $\theta=\pi/2$, the Bragg gap shrinks a little and a quite wide non-Bragg gap appears. In the case of the antisymmetric arrangement ($\theta=\pi$), we observe that the surface wave propagates without the Bragg reflection, but it can suffer much stronger non-Bragg reflection in an impressively wide band gap.

As compared with the predictions in Fig. 3, we notice that the measured results in Fig. 5 indicate some additional transmission loss (over 5 dB in the frequency range), and this loss tends to be greater at higher frequency. We ascribe this wave attenuation to the damping effect which is inevitable in experiment. Generally speaking, the damping effect becomes strong as the frequency f increases. Actually, for the water waves ($ka\approx0.2$) considered here, the viscous coefficient of water $\nu=0.01$ cm^2/s, and the Reynold's number $R=\omega a/(k\nu)$ [37], is estimated to decrease from 6300 to 1500 as the frequency increases from 2.30 to 3.75 Hz.

In addition to the damping effect, we also notice that all non-Bragg gaps shift a bit toward higher frequency. Presumably, this difference might be caused by the meniscus on the sidewalls. The contact line can move and the maxima of the water surface are not located at the walls. In the experiments, the "effective" width of the trough is smaller than b, which means a higher frequency for the non-Bragg reflections [19]. Aside from these discrepancies, we see that the experimental

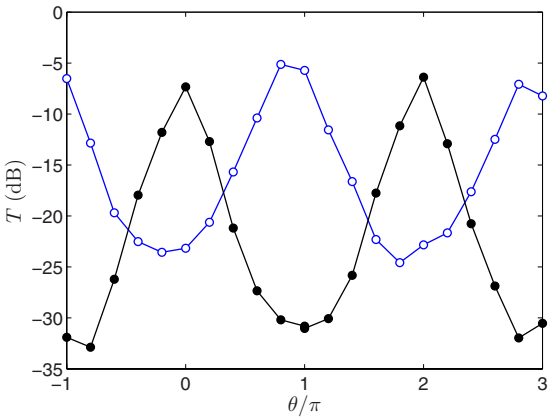

FIG. 6. (Color online) Measured transmission coefficients T vs phase shift θ at $f=2.80$ (the line-connected empty circles) and 3.20 Hz (the line-connected black circles)

results agree fairly well with the numerically computed ones.

To further understand the non-Bragg resonance, let us examine how the transmission coefficient T varies with the phase shift θ in more detail. Shown in Fig. 6 are the results for two selected frequencies $f=2.80$ and 3.20 Hz, which are located, respectively, within the Bragg and non-Bragg gaps (see Fig. 5). Clearly, T is a periodic function of θ with period 2π, i.e., $T(\theta+2\pi)=T(2\pi)$, but the two functions for $f=2.80$ and 3.20 Hz are exactly π out of phase, which is in agreement with the predictions in Sec. III. At the lower frequency, only the Bragg resonance can be observed by varying the phase shift, and the maximum transmission loss occurs for $\theta=2n\pi$, $n=0,\pm1,\pm2,\ldots$. On the contrary, at the higher frequency, only the non-Bragg resonance can occur, and the resulting transmission loss becomes maximum at $\theta=n\pi$, $n=\pm1,\pm3,\ldots$.

V. CONCLUSIONS

In conclusion, we have performed both theoretical and experimental investigations on surface-wave propagation in a trough with periodically corrugated sidewalls and explored the existence of a resonance of non-Bragg nature in addition to the well-known Bragg resonance. By invoking the plane-wave expansion, a numerical method is developed to analyze the resonance-induced band gaps. Both Bragg and non-Bragg gaps are predicted theoretically and then confirmed experimentally. Unlike the Bragg resonance, the non-Bragg one occurs between modes of different transverse wave profiles, and thus it manifests itself in some higher frequency range. We also find that, in the present wave system, the resonance can occur only if there is a nontrivial phase shift θ in the periodicity of the opposite sidewalls, while the usual Bragg resonance favors the symmetrical wall configuration with respect to the midline of the water channel. As the phase shift θ goes from 0 (symmetrical) to π (antisymmetrical), the Bragg resonance becomes weak and then disappears, while the non-Bragg resonance appears and becomes dominant in reflecting incident waves. Accordingly, the Bragg band gap shrinks in the lower frequency range, but the non-Bragg band gap expands in the higher frequency range. Therefore, both band gaps are highly tunable by the phase shift.

Unexpectedly, the observed maximal non-Bragg gap (at $\theta=\pi$) is impressively wide, and the transmission loss inside this gap is much greater, showing the crucial role the non-Bragg resonance plays in water wave propagation in such a periodic water channel. In the intermediate case, $0<\theta<\pi$, both Bragg and non-Bragg resonances contribute to the resulting band structure. All these interesting findings will not only benefit the understanding of wave propagation in complex waveguides, but also open a broad scenario to design more complex band structures in such applications as ocean engineering.

ACKNOWLEDGMENTS

This work is supported by the National Science Foundation of China under Grants No. 10604031 and No. 10474045, and by the Research Fund for the Doctoral Program of Higher Education of China.

[1] T. Opatrny, B. A. Malomed, and G. Kurizki, Phys. Rev. E **60**, 6137 (1999).
[2] S. Suntsov, K. G. Makris, D. N. Christodoulides, G. I. Stegeman, A. Hache, R. Morandotti, H. Yang, G. Salamo, and M. Sorel, Phys. Rev. Lett. **96**, 063901 (2006).
[3] F. R. MonterodeEspinosa, E. Jimenez, and M. Torres, Phys. Rev. Lett. **80**, 1208 (1998).
[4] S. Yang, J. H. Page, Z. Liu, M. L. Cowan, C. T. Chan, and P. Sheng, Phys. Rev. Lett. **93**, 024301 (2004).
[5] W. Liang, Y. Huang, Y. Xu, R. K. Lee, and A. Yariv, Appl. Phys. Lett. **86**, 151122 (2005).
[6] B. Li, L. Wang, and G. Casati, Phys. Rev. Lett. **93**, 184301 (2004).
[7] B. Li, J. Lan, and L. Wang, Phys. Rev. Lett. **95**, 104302 (2005).
[8] D. Janner, G. Galzerano, G. DellaValle, P. Laporta, S. Longhi, and M. Belmonte, Phys. Rev. E **72**, 056605 (2005).
[9] L. Feng, X.-P. Liu, M.-H. Lu, Y.-B. Chen, Y.-F. Chen, Y.-W. Mao, J. Zi, Y.-Y. Zhu, S.-N. Zhu, and N.-B. Ming, Phys. Rev. Lett. **96**, 014301 (2006).
[10] A. G. Davies and A. D. Heathershaw, J. Fluid Mech. **144**, 419 (1984).
[11] C. C. Mei, J. Fluid Mech. **152**, 315 (1985).
[12] J. T. Kirby, J. Fluid Mech. **162**, 171 (1986).
[13] Y. Liu and D. K. P. Yue, J. Fluid Mech. **356**, 297 (1998).
[14] Y.-M. Xiao, Z.-Y. Tao, and X.-L. Wang, Chin. Phys. Lett. **23**, 1846 (2006).
[15] R. Porter and D. Porter, J. Fluid Mech. **434**, 301 (2001).
[16] Z. Ye, Phys. Rev. E **67**, 036623 (2003).
[17] Z. An and Z. Ye, Appl. Phys. Lett. **84**, 2952 (2004).

[18] Y.-K. Ha, J.-E. Kim, and H. Y. Park, Appl. Phys. Lett. **81**, 1341 (2002).
[19] T. S. Jeong, J.-E. Kim, and H. Y. Park, Appl. Phys. Lett. **85**, 1645 (2004).
[20] V. P. Ruban, Phys. Rev. E **70**, 066302 (2004).
[21] Y. Li and C. C. Mei, Phys. Rev. E **76**, 016302 (2007).
[22] M. Torres, J. P. Adrados, and F. R. M. de Espinosa, Nature (London) **398**, 114 (1999).
[23] M. Torres, J. P. Adrados, F. R. MonterodeEspinosa, D. Garcia-Pablos, and J. Fayos, Phys. Rev. E **63**, 011204 (2000).
[24] X. Hu, Y. Shen, X. Liu, R. Fu, and J. Zi, Phys. Rev. E **68**, 066308 (2003).
[25] X. Hu, Y. Shen, X. Liu, R. Fu, and J. Zi, Phys. Rev. E **69**, 030201(R) (2004).
[26] Y. Shen, K. Chen, Y. Chen, X. Liu, and J. Zi, Phys. Rev. E **71**, 036301 (2005).
[27] V. A. Pogrebnyak, Phys. Rev. E **58**, R5261 (1998).
[28] V. A. Pogrebnyak, Phys. Rev. B **69**, 245307 (2004).
[29] V. A. Pogrebnyak, Opt. Commun. **232**, 201 (2004).
[30] In a waveguide, the term "transverse modes" refers to those two-dimensional surface-wave modes that have distinct standing-wave profiles transverse to the waveguide axis or the direction of wave propagation.
[31] V. A. Pogrebnyak, E. Akray, and A. N. Kucukaltun, Appl. Phys. Lett. **86**, 151115 (2005).
[32] L.-F. Philip and Liu, J. Fluid Mech. **179**, 371 (1987).
[33] E. S. Benilov and M. I. Yaremchuk, Wave Motion **13**, 115 (1991).
[34] W. D. McKee, Appl. Ocean. Res. **21**, 145 (1999).
[35] Z. Y. Tao, Y. M. Xiao, and X. L. Wang, Chin. Phys. Lett. **22**, 394 (2005).
[36] O. Z. Zienkiewicz and R. L. Taylor, *The Finite Element Method*, 5th ed. (World Scientific, Beijing, 2005).
[37] C. C. Mei, *The Applied Dynamics of Ocean Surface Waves* (World Scientific, Singapore, 1989).